Astron. Astrophys. 309, 705–714 (1996)

ASTRONOMY
AND
ASTROPHYSICS

Molecular distribution and kinematics in nearby galaxies

II. Sub-mm observations of NGC 4945*

R. Mauersberger[1,2], C. Henkel[1], J.B. Whiteoak[3], Y.-N. Chin[4], and A.R. Tieftrunk[1]

[1] Max-Planck-Institut für Radioastronomie, Auf dem Hügel 69, D-53121 Bonn, Germany
[2] Steward Observatory, The University of Arizona, Tucson, AZ 85721, USA
[3] Australia Telescope National Facility, CSIRO Radiophysics Lab., P.O., Box 76, Epping, NSW 2121, Australia
[4] Radioastronomisches Institut der Universität Bonn, Auf dem Hügel 71, D-53121 Bonn, Germany

Received 22 August 1995 / Accepted 13 October 1995

Abstract. The central $80'' \times 80''$ of the nearby edge-on starburst galaxy NGC 4945 has been mapped in the $J = 3-2$ line of ^{12}CO with a resolution of 15″. Spectra of the $J = 3-2$ transition of ^{13}CO and tentative detections of the $J = 4-3$ line of HCN and the $J_{K_aK_c} = 3_{12} - 2_{11}$ line of H_2CO are also presented. The CO $J = 3-2$ emission is concentrated toward the kinematical center of the galaxy with a deconvolved full width at half power (FWHP) size of $(11.5\pm3)''$ corresponding to (200 ± 50) pc at a distance $D = 3.7$ Mpc. This is less than the extent of the nuclear molecular complex as derived from the distributions of the lower rotational CO transitions. Position-velocity maps reveal three condensations located at the center and at offsets of 5″ toward either side of the nucleus. The dynamical mass in the inner $R \leq 600$ pc is $\sim 3\,10^9$ M$_\odot$.

Applying a "standard" $N(H_2)/I(CO)$ conversion factor of $2\,10^{20}$ cm^{-2}/(K km s^{-1}), the central molecular gas mass is $\sim 9\,10^8$ M$_\odot$. Like in the case of the central regions of the Milky Way and NGC 253, integrated ^{12}CO line intensities combined with a standard conversion factor yield a gas mass which is 6 to 14 times higher than that obtained from multi-transition CO models and from the dust continuum emission. If the latter results are correct, we find a conversion factor of only 0.15–0.35 10^{20} cm^{-2}/(K km s^{-1}) for the central region of NGC 4945. An embedded active nucleus may contribute to the very high "star forming efficiency" $L_{IR}/M_{gas} \sim 140$ L$_\odot$/M$_\odot$. The contribution of the CO lines to the "continuum" flux density in a 50 GHz 1.3 mm band is comparable to that of the dust. From the strength of the CO $J = 3-2$ emission and our tentative detection of high density tracing molecules, the bulk of the CO emitting gas should have a high density ($n(H_2) = 10^{3.5}$– 10^4 cm^{-3}) and is clumped with a beam filling factor of roughly 20%.

Key words: galaxies: individual: NGC 4945 – galaxies: starburst – galaxies: ISM – galaxies: nuclei – ISM: clouds

1. Introduction

NGC 4945 is a nearly edge-on ($i = 78°$; Ott 1995) southern galaxy with an optical size of almost 0.5° and a distance of ~ 3.7 Mpc (see Sect. 4.1). Intense infrared and radio emission is observed from its nuclear region (Mills & Glanfield 1965, Whiteoak & Gardner 1979, Brock et al. 1988, Rice et al. 1988, Ghosh et al. 1992). Nearly all the far-infrared luminosity of $\sim 2\,10^{10}$ L$_\odot$ comes from a nuclear source of size $12'' \times 9''$ (220 pc $\times$ 160 pc; Brock et al. 1988). NGC 4945 is also one of the most prolific extragalactic sources for high-density tracing molecules (Henkel et al. 1990, 1994). It has been suggested that NGC 4945 is in a post-starburst phase (Koornneef 1993) or in a transition from a starburst to a Seyfert galaxy (Moorwood & Oliva 1994). The presence of a Seyfert nucleus has been inferred from X-ray observations (Iwasawa et al. 1993).

The large scale distribution of the gas in NGC 4945 has been previously mapped in the $J = 1-0$ line of ^{12}CO (Whiteoak et al. 1990, Dahlem et al. 1993) as well as in H I (Ables et al. 1987) and the CO $J = 2-1$ line (Ott 1995). Kinematic information and the measured line intensities indicated the presence of a spatially unresolved molecular ring. Comparing the profiles of different CO isotopes, Bergman et al. (1992) predicted that this ring should consist of low density clumps. This was questioned by Henkel et al. (1994) on the basis of observations of high density tracing molecules. They suggested a different spatial origin of molecular lines with different excitation conditions.

In order to estimate distribution and kinematics of the molecular gas component in the center of NGC 4945 with high angular resolution, we have used the Swedish-ESO Sub-mm Telescope (SEST; see Booth et al. 1989) to map ^{12}CO in its $J = 3-2$

Send offprint requests to: R. Mauersberger, Steward Observatory

* Based on observations with the Swedish-ESO sub-millimeter telescope, SEST, ESO/La Silla, Chile

transition. Additional SEST data from ^{13}CO, HCN, and H_2CO will also be analysed.

2. Observations

The $J = 3-2$ lines of ^{12}CO ($\nu = 345.7960$ GHz) and ^{13}CO ($\nu = 330.5880$ GHz) were observed with the SEST in May and July 1993 and in May 1994. In May 1994, we also obtained spectra of the $J = 4-3$ transition of HCN ($\nu = 354.4055$ GHz; total integration time, $t_{\rm int}$, 160 minutes), and of the $J_{K_aK_c} = 3_{1,2} - 2_{1,1}$ transition of H_2CO ($\nu = 225.6989$ GHz; $t_{\rm int}$ =260 minutes).

NGC 4945 was mapped on a raster tilted by 43 degrees with respect to right ascension and declination, for alignment with the major axis, and centered on a nominal position of the galactic nucleus of $\alpha_{1950} = 13^{\rm h}02^{\rm m}32\overset{\rm s}{.}2$, $\delta_{1950} = -49°12'02''$. The raster in the ^{12}CO line (measured in one session in May 1993) consists of 9×9 positions with a spacing of 10″. Map center and spacing are the same as for the SEST ^{12}CO $J = 2-1$ map taken by Dahlem et al. (1993) with an angular resolution of 43″. The total on-source integration time for each position was 2 minutes. In July 1993, we additionally measured 9 positions with 5″ spacing along the major axis and centered on the nominal map origin with 4 minutes integration time per point. In May 1994 we repeated the map of the central part of NGC 4945 on a finer grid with 7″ spacing and 5 × 7 raster positions. In July 1993 and May 1994, we observed ^{13}CO $J = 3-2$ at five positions along the major axis with a separation of 5″ and with total integration times between 6 and 30 minutes per point.

The FWHP beamwidth of the SEST was 15″, 23″ and 45″ at 330—354 GHz, 225 and 115 GHz, respectively (SEST-Handbook 1993). For the observations at 330—354 GHz, an SIS receiver was used with a receiver temperature of 320 K; this and favorable weather conditions (zenith opacities, $\tau_z \leq 0.3$) led to system temperatures, $T_{\rm sys}$, of 400 to 700 K (elevations were always between 45° and 69°). At 354 GHz, $T_{\rm sys}$ was 1100 K. Antenna temperatures "outside the Earth's atmosphere" ($T_{\rm A}^*$) are used which are based on a chopper wheel calibration (for conversion to main-beam brightness temperature, see Sect. 3.4). For the H_2CO line, a 1.3 mm SIS receiver has been employed, yielding a $T_{\rm sys}$ of $\sim$ 850 K (see the SEST-Handbook 1993 for details).

For the line observations we used a "dual beam-switch" mode with a beam-throw of 11′40″ in azimuth. The source was first placed in the signal beam and then in the reference beam. Combining such pairs of spectra yielded flat baselines. The backends used were acousto-optical spectrometers (AOS) with resolutions of 1.4 MHz and total bandwidths of 995 and 1086 MHz (corresponding to 865 and 944 km s^{-1} at 345 GHz).

Radial focusing of the receiver was obtained by measuring planets at the beginning of each observational period. The pointing of the telescope was determined by measuring 5-point rasters of the 3 mm continuum of Centaurus A, which is close to NGC 4945 on the sky. The telescope control program automatically corrected for the misalignment between the 3 mm receiver used for pointing and the 345 GHz SIS receiver, which had been determined by the SEST staff. Successive pointings with the 3 mm receivers in the May 1993 session yielded differences in the pointing offsets in order 5″. These fluctuations might be caused by anomalous refraction (see e.g. Altenhoff et al. 1987), wind, or from the raster pointing procedure. A comparison between the pointings at the beginning and at the end of the line observations in May 1993 (elapsed time: $4^{\rm h}30^{\rm m}$) shows that the pointing offsets had changed by 10″. This is also the maximum uncertainty of the positions given. For those raster lines with $\Delta y = 0''$, $\pm10''$ and $\pm20''$ in the descriptive system, which contain the strongest line emission, pointing errors are probably smaller than 10″, since those points were measured in the beginning of the run. In summary, we estimate pointing errors are $\sim 5'' - 7''$ in the central region, where strong line emission is observed. The uncertainty is 10″ for the regions with $\Delta y = \pm30''$, $\pm40''$, where line emission is weak. There is an excellent agreement in the lineshapes for the profiles at the central positions obtained in May 1993 and May 1994. In view of the rapid change in line profiles with position we estimate that both maps are aligned within 4″.

Linear baselines were subtracted from all the profiles. For the presentation, the velocity resolution of the spectrometer has been reduced.

3. Results

3.1. The profiles

Fig. 1a-c presents the ^{12}CO $J = 3-2$ profiles measured toward the central region of NGC 4945. CO (3−2) emission is strongly concentrated toward the inner 20—30 arcseconds, but weak emission is observed over the whole mapped region, as can be seen from Fig. 1b. Maximum $T_{\rm A}^*$ values for CO are about 1.4 K. Emission arises from a velocity range of $\sim 300 - 750$ km s^{-1}. Intensities and line shapes of the nuclear emission are not symmetrical with respect to our (0″,0″) position.

In Fig. 1d, we present ^{13}CO $J = 3-2$ profiles along the major axis of NGC 4945. The $J = 4-3$ line of HCN and the $J_{K_aK_c} = 3_{12} - 2_{11}$ transition of H_2CO together with the central profile of CO $J = 3-2$ are shown in Fig. 2.

In both the HCN and H_2CO spectra there may be faint emission at 400–500 km s^{-1}, where the CO emission is strongest. A Gaussian fit to the H_2CO line yields $\int T_{\rm A}^* {\rm d}v = 1.4(0.7)$ K km^{-1}, $v_{\rm LSR} \sim 420$ km s^{-1}, and $\Delta v_{1/2} \sim 160$ km s^{-1} (FWHP), i.e. the signal is only twice the formal error. For HCN, we have fixed the linewidth and velocity to the values obtained from a Gaussian fit to the ^{12}CO line ($v_{\rm LSR}$ = 487 km s^{-1}, $\Delta v_{1/2}$ = 196 km s^{-1}), and obtain an integrated intensity of $\int T_{\rm A}^* {\rm d}v$=1.7(0.6) K km s^{-1}, i.e. a 3σ "detection". This is a much lower limit than the value of $\sim$ 50 K km s^{-1} estimated by Jackson et al. (1995) from CSO (CalTech Submillimeter Observatory) observations of HCN $J = 4-3$ toward NGC 4945.

3.2. The CO $J = 3-2$ contour map

In Fig. 3, we show a contour map of the integrated intensity of the CO emission. We have fitted a two-dimensional Gaussian to the distribution of $\int T_{\rm A}^* {\rm d}v$ with a resulting FWHP of $28'' - 29''$;

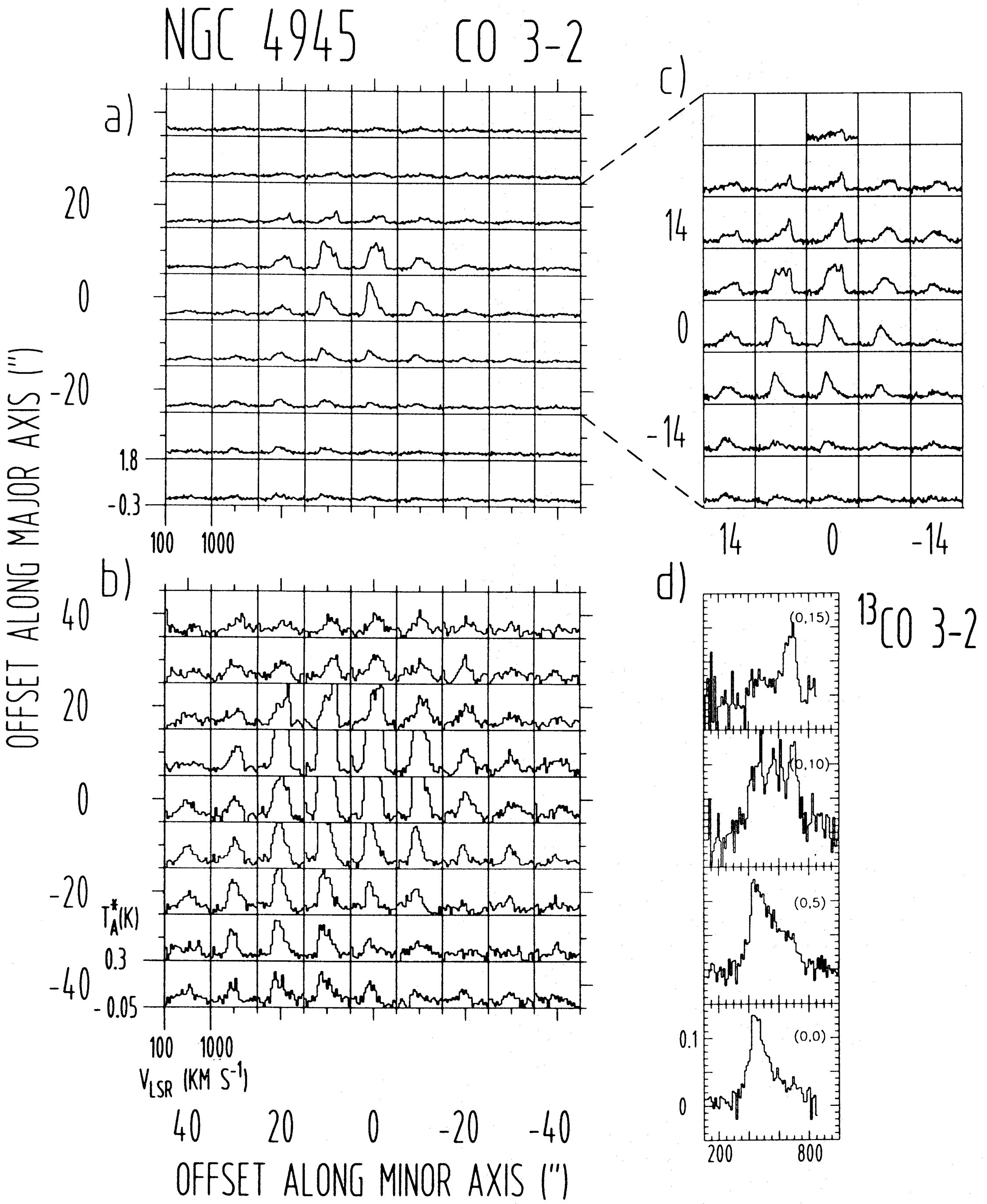

Fig. 1a–d. Map of the CO $J = 3-2$ profiles measured toward the center of NGC 4945. The offsets are given with respect to a nominal position of $\alpha_{1950} = 13^h02^m32\overset{s}{.}2$, $\delta_{1950} = -49°12'02''$, and the major axis of the galaxy (P.A. = 43°). The T_A^* scale and the velocity scale (with respect to the Local Standard of Rest) are given at the lower left frame. Add 5 km s^{-1} to obtain heliocentric velocities, v_{hel}. **a** The ^{12}CO $J = 3-2$ map obtained in May 1993. The spacing is 10''. The velocity resolution has been degraded to 12 km s^{-1}. **b** The same spectra, but with an enlarged intensity scale to show the weak, extended emission. The velocity resolution has been smoothed to 36 km s^{-1}. **c** For comparison, the map obtained in May 1994 is shown. The spacing is 7'', the velocity resolution is 12 km s^{-1}. **d** ^{13}CO $J = 3-2$ profiles measured toward four positions along the major axis (velocity resolution: 12 km s^{-1}).

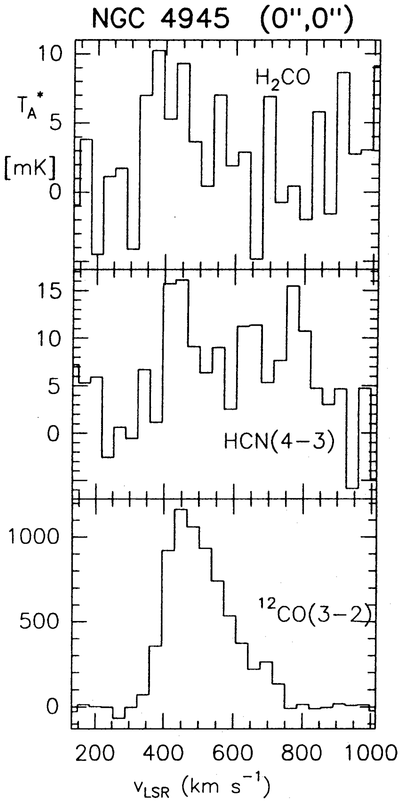

Fig. 2. $J = 4-3$ and $J_{K_aK_c} = 3_{12} - 2_{11}$ spectra of HCN and H_2CO together with the ^{12}CO $J = 3-2$ profile toward the $(0'', 0'')$ position. The velocity resolution is $36\,km\,s^{-1}$.

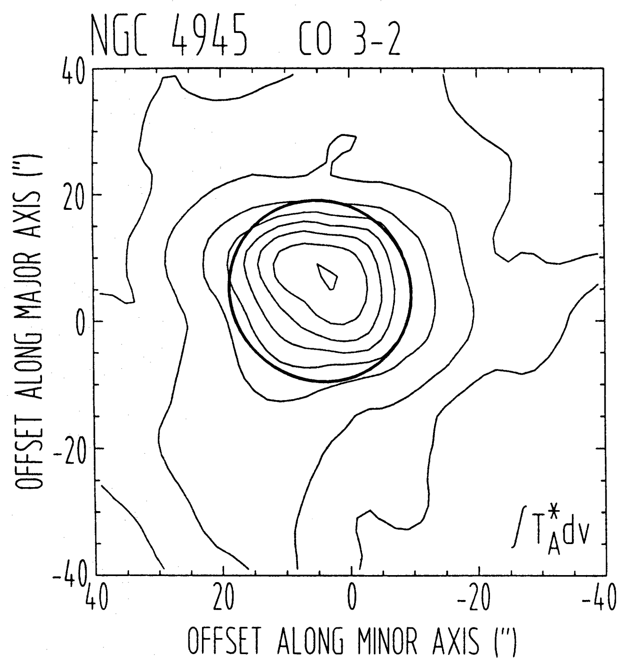

Fig. 3. A contour map of the integrated CO (3 − 2) line emission, $\int T_A^* dv$, toward the center of NGC 4945. The data were taken in May 1993. (The contour map obtained in May 1994 looks very similar.) Contours are 25, 50, 100, 150... $K\,km\,s^{-1}$. The overlayed ellipse denotes the FWHP of a two-dimensional Gaussian fit to the data.

the center of the Gaussian is at $(\Delta x, \Delta y) = (5'', 5'')$ for both data sets (i.e. from May 1993 and May 1994), corresponding to a position of $\alpha_{1950} = 13^h02^m32\overset{s}{.}9$, $\delta_{1950} = -49°12'02''$. This is an offset of $6''$ from the position of the radio nucleus ($\alpha_{1950} = 13^h02^m32\overset{s}{.}34$, $\delta_{1950} = -49°12'00\overset{''}{.}5$; Whiteoak & Wilson 1990). Within the uncertainties due to the pointing errors, our beam size and the spatial sampling the molecular center of NGC 4945 coincides with the radio nucleus.

Due to a more extended underlying emission component, the width from a Gaussian fit overestimates the size of the central condensation. Therefore, we have made cuts through the center of the ellipse shown in Fig. 3. From these cuts, the width of the central condensation alone is $22''(\pm 2'')$. Deconvolved with the beamwidth of $15''$ and accounting for the raster spacing $(10'')$, this yields an intrinsic size of the central condensation of $11''(\pm 4'')$. A similar analysis of the data obtained in May 1994 yields an undeconvolved size of $20\overset{''}{.}5 \pm 2\overset{''}{.}5$, and the deconvolved size of the central condensation becomes $12'' \pm 4''$. We conclude that from both maps the size (FWHP) of the central molecular complex is $11\overset{''}{.}5 \pm 3''$ (220 pc±60 pc). We compile the source sizes derived from the emission of the $J = 1-0$ to $3-2$ lines by Dahlem et al. (1993) and by us in Table 1.

Table 1. FWHP size of the central peak in CO emission

Line	Apparent width[a] ($''$)	Beam ($''$)	Raster spacing[a] ($''$)	Deconvolved size[a,b] ($''$)	(pc)
$1-0^c$	54(2)	43	20	26(5)	470(90)
$2-1^c$	32(2)	24	10	18(5)	320(90)
$3-2^d$	22(2)	15	7 − 10	11.5(3)	200(55)

a) FWHP; the values in parentheses are the estimated standard deviations

b) Note that the sizes quoted by Dahlem et al. (1993) are not deconvolved for the raster spacing. While Dahlem et al. (1993) assumed a distance of 6.7 Mpc, values in this table are based on a distance of 3.7 Mpc

c) Dahlem et al. (1993)

d) This paper

3.3. The velocity structure

Fig. 4 shows the intensity distribution at various velocities, integrated over a range of $48\,km\,s^{-1}$. While the position where maximum emission occurs changes only by $9''$ (160 pc), the radial velocities shift from $v_{LSR} = 390\,km\,s^{-1}$ to $730\,km\,s^{-1}$ along the major axis. Due to this high velocity gradient, the sizes of the emitting regions at a given velocity should be smaller than those determined from the map of integrated intensity.

Position velocity plots along the major axis are shown in Fig. 5. The combined data of May/July 1993 and the data obtained in May 1994 show not only the same features but the agreement in line intensities is also good. Thus all features

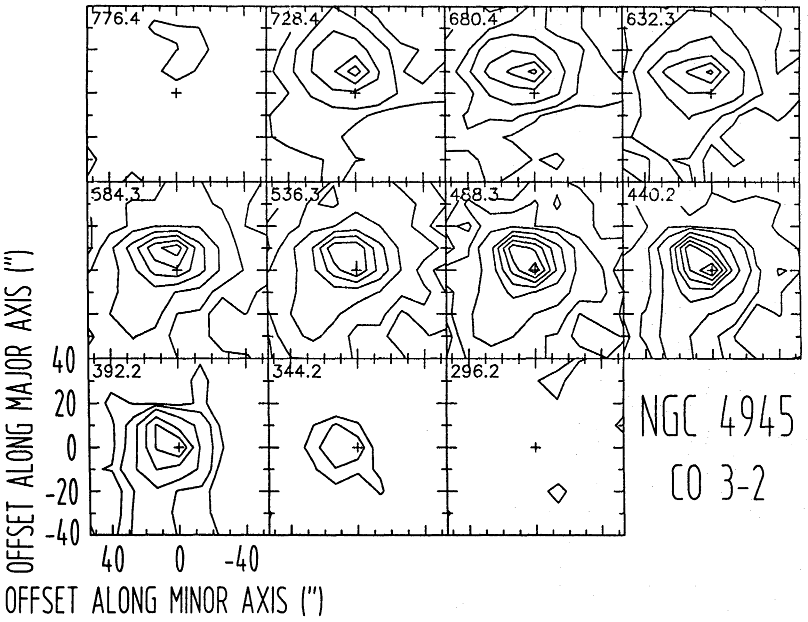

Fig. 4. Maps of integrated intensity, $\int T_{\rm A}^{*} {\rm d}v$, in $48\,{\rm km\,s^{-1}}$ wide channels (data from May 1993). Contour levels are 2.5, 5, 10, 20, 30... $\rm K\,km\,s^{-1}$.

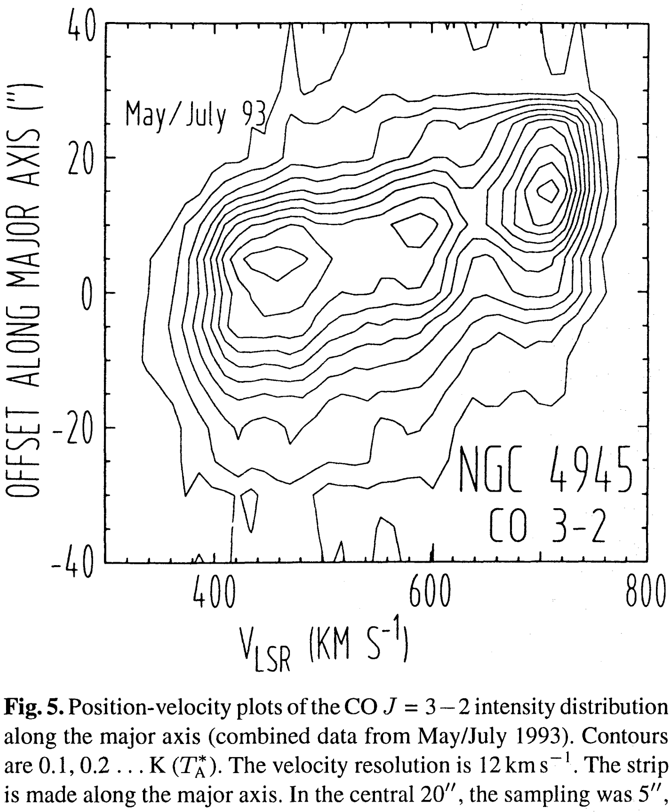

Fig. 5. Position-velocity plots of the CO $J = 3-2$ intensity distribution along the major axis (combined data from May/July 1993). Contours are 0.1, 0.2 ... K ($T_{\rm A}^{*}$). The velocity resolution is $12\,{\rm km\,s^{-1}}$. The strip is made along the major axis. In the central 20″, the sampling was 5″, in the outer parts 10″.

can be considered as real. From the plots, we can distinguish three spatially unresolved or marginally resolved maxima, at velocities of 460 (in the 1993 data set at a major axis offset of Δy = 4″), 590 (at Δy = 8″) and $700\,{\rm km\,s^{-1}}$ (at Δy = 15″). In the 1994 data, the positions are shifted 3″ toward lower offsets values. Toward the maxima, the FWHP linewidths are between $\sim$ 80 (for the $700\,{\rm km\,s^{-1}}$ component) and $\sim 120\,{\rm km\,s^{-1}}$ (for the $460\,{\rm km\,s^{-1}}$ component).

3.4. ^{12}CO line intensity ratios

More significant for physical studies than $T_{\rm A}^{*}$ is the main-beam brightness temperature, $T_{\rm MB}$, which, in essence, is the Rayleigh-Jeans brightness temperature of the source averaged over the beam, if the source size is not much larger than the beam. The main-beam brightness temperature can be obtained using the relation $T_{\rm MB} = T_{\rm A}^{*}/\eta_{\rm MB}$ (SEST-Handbook), with the main-beam efficiency $\eta_{\rm MB}$ = 0.25, 0.60 and 0.70 at 345, 225 and 115 GHz respectively. Particularly at the highest frequencies, the contribution from the error-beam can be significant (L.-Å. Nyman, priv. comm.; see also the discussion in García-Burillo et al. 1993) if the source size is larger than the beam. While the CO $2-1$ line emission is strongly concentrated toward the inner 30″ of NGC 4945, there is also weaker emission over an area of $2' \times 12'$, which is picked up by the error beam. We think, however, that $T_{\rm MB}$ is the most suitable intensity scale because (1) there is probably much less contribution from extended J=3-2 line emission than from the $2-1$ line and (2) for a given velocity channel the emission may arise from a *much* smaller size than if one measures the integrated line intensity. An inspection of Fig. 4 of Dahlem et al. (1993) shows that the extended CO emission arises mainly at $750\,{\rm km\,s^{-1}}$ and at $380\,{\rm km\,s^{-1}}$, while velocity components between 450 and $650\,{\rm km\,s^{-1}}$ are much more concentrated toward the center.

In order to compare the line intensities of different rotational lines of ^{12}CO, we converted our data and the data of Dahlem et al. (1993) to a main-beam brightness temperature scale. We then convolved our $J = 3-2$ map to resolutions of 24″ and 43″; the data from Dahlem et al. were also convolved to a 43″ resolution. In Fig. 6a, we compare all three lines toward our map origin at a resolution of 43″, and in Fig.6b, we compare the $3-2$

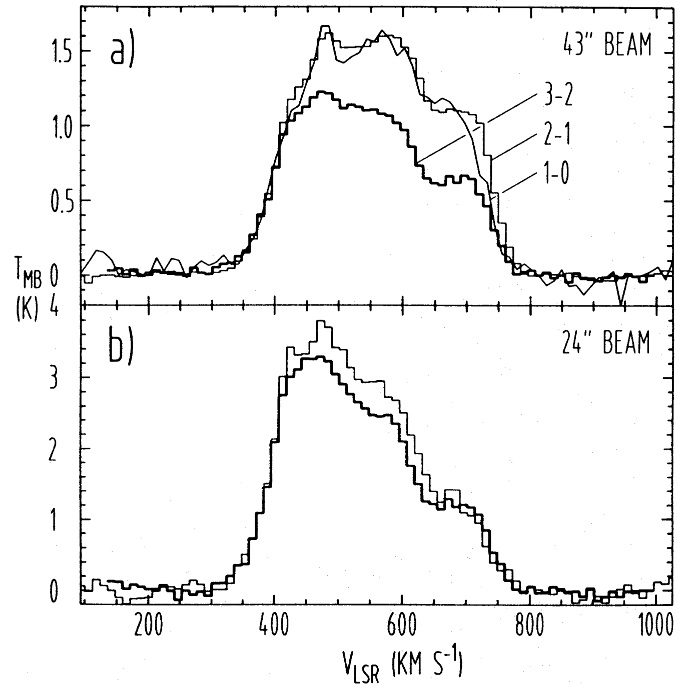

Fig. 6. a The lowest three rotational CO lines toward the central position convolved to a resolution of 43″. **b** The $J = 2-1$ and $3-2$ lines convolved to a 24″ beam.

Table 2. CO line intensities toward the center of NGC 4945

	Resol. (″)	$\int T_{\rm MB} {\rm d}v$ K km s^{-1} (1 − 0)	(2 − 1)	(3 − 2)
^{12}CO	15			950
	24	(850)[c]	910[a]	800
	43	450	480[a]	340
^{13}CO	15			90
	24	(60)[c]	100[b]	(80)[c]
	43	32[b]		
$\frac{I(^{12}\rm CO)}{I(^{13}\rm CO)}$		14[d]	8.8[e]	10.5[f]

a) data by Dahlem et al. (1993)
b) Henkel et al. (1994); the beam efficiencies cited in Sect. 3.4 were applied to convert to $T_{\rm MB}$.
c) values in brackets were estimated from the line ratios at 43″ resolution or the mean ^{12}CO/^{13}CO ratio.
d) beam size 43″
e) beam size 24″
f) beam size 15″

line with the $2-1$ line at a resolution of 24″. It is evident that the $2-1$ and $3-2$ lines have virtually the same shape and intensity when observed with a 24″ beam (The asymmetry of the line shape reflects the slight offset of the molecular center from our map origin.) With a resolution of 43″, however, the $3-2$ line is weaker than both the $2-1$ and $1-0$ lines, which are nearly identical in shape and intensity. To quantify this, we list the integrated intensities of the various lines in Table 2.

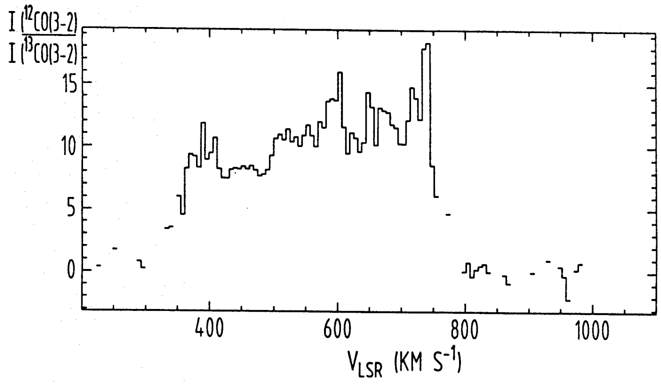

Fig. 7. The ^{12}CO$(3-2)/^{13}$CO$(3-2)$ intensity ratio as function of velocity. The spectra used to determine the ratio are averages of measurements toward the $\Delta y = 0''$, $5''$ and $10''$ offsets, in order to allow for a better comparison with $J = 1-0$ and $2-1$ data and to be less sensitive to pointing errors. Channels are not plotted if the denominator channel has an absolute intensity below the rms noise level.

3.5. The ^{12}CO/^{13}CO intensity ratio

We also display the ^{12}CO/^{13}CO intensity ratios for the $1-0$, $2-1$ and $3-2$ lines in Table 2. These ratios are between $\sim$ 10 and 14. The velocity dependence of the ratio for the $(3-2)$ lines is shown in Fig. 7. In order to avoid the influence of small pointing errors, we have averaged over three positions where CO emission is strongest. It is possible that the ratio is slightly smaller near 400 km s^{-1}, namely $\sim$ 9, than between 600—750 km s^{-1}, where it is 12, but this can also be mimicked by a small pointing offset between the ^{12}CO and ^{13}CO spectra.

4. Discussion

4.1. The distance to NGC 4945

Although much attention has been paid to NGC 4945, in particular by infrared and radio astronomers, little is known about its distance. Van den Bergh (1989) summarizes efforts to estimate the distance of the NGC 5128/5236 (i.e. Cen A/M 83) group of galaxies to which NGC 4945 appears to belong. The three galaxies share the mean cluster radial velocity (Hesser et al. 1984), and are possibly at a comparable distance.

While earlier estimates of the distance to NGC 5128 (Cen A) show a large scatter (Sandage & Tammann 1975: 7.9 Mpc, de Vaucouleurs 1979: 3.3 Mpc), more recent values seem to converge. Comparing the globular cluster luminosity functions of Cen A with those of the Galaxy and M 31, Harris et al. (1986) obtain a distance of 3.2 Mpc, with considerable uncertainty. $D = (3.5 \pm 0.2)$ Mpc is obtained when using Tonry & Schechter's (1990) results applying a surface brightness fluctuation technique (SBF) combined with a revised calibration (Tonry 1991, Hui et al. 1993). Ruiz-Lapuente & Lucy (1992) estimate $D = (3.3 \pm 0.3)$ Mpc from the analysis of nebular lines toward a Type Ia supernova in Cen A. Hui et al. (1993) used planetary nebulae toward Cen A as a standard candle and also estimated $D = (3.5 \pm 0.2)$ Mpc.

Sandage et al. (1994) used the Hubble Space Telescope to determine the distance toward NGC 5253 and obtain $D = (4.1 \pm 0.1)$ Mpc, which is consistent with recent values deduced from the Type Ia supernova SN 1972 E (Della Valle & Melnick 1992: $D = (4.6 \pm 0.7$ Mpc) and the SBF technique (Shopbell et al. 1993: $D = (3.8 \pm 0.1)$ Mpc).

To summarize, distances for members of the Centaurus cluster range between 3.5 Mpc for Cen A and 4.0 Mpc for NGC 5253. Here we will assume a value of 3.7 Mpc. At this distance, $1''$ corresponds to 18 pc. Gas mass and luminosity estimates based on the often cited distance of 6.7 Mpc (e.g. Whiteoak & Gardner 1977) must be multiplied by a factor of 0.30 before being compared with estimates from this study; dynamical masses have to be multiplied by a factor of 0.55.

4.2. Distribution and kinematics of the circumnuclear gas

The nuclear cloud shows a remarkable decrease in size when going from the lower ^{12}CO transitions to the ^{12}CO $3-2$ line, and seems to be nearly unresolved with our $15''$ beam (see Table 1). In all cases, however, the source size is slightly smaller than the applied beam size, and there is, within the limits of uncertainty, some overlap in the estimates of the extent of the $J = 2-1$ and the $3-2$ CO emission. Although NGC 4945 is seen nearly edge-on, there is no elongation or preferred direction from the $J = 3-2$ contour maps (Fig. 3), except perhaps some weak emission along the major axis. While the size of the $J = 1-0$ and $2-1$ emission is comparable with the region of Fe II and H_2 emission (Moorwood & Oliva 1994), the source size of the ^{12}CO $J = 3-2$ emission is similar to the size of the far infrared emission (FIR) of $12'' \times 9''$ (Brock et al. 1988). We will assume that the FIR and CO $3-2$ emission arise from the same region.

Where large systematic velocity gradients are present, position velocity plots (Fig. 5) can resolve spatial structure which is smaller than the telescope beam. As already mentioned, the maximum emission changes merely by $\sim 9''$ along the major axis (i.e. 160 pc), if one goes from a velocity as high as 728 km s^{-1} to a velocity as low as 392 km s^{-1} (Fig. 4). For the same difference in velocity, a shift of $\sim 18''$ is observed along the major axis of NGC 253 (Mauersberger et al. 1996, hereafter Paper I), corresponding to a distance of 220 pc at $D = 2.5$ Mpc. If NGC 253 and NGC 4945 were at the same distance, the molecular gas distributions as well as the CO distribution in individual channel maps would look similar. There remains however one striking difference: While the central region of NGC 253 contains two CO maxima separated by $16''$, a redshifted and a blueshifted one, there are three maxima seen toward the central region of NGC 4945 (Sect. 3.3 and Fig. 5), one redshifted, one blueshifted, and a third, central maximum at the systemic velocity. These have been identified in two independent data sets.

A double molecular structure of two concentric rings with $5\farcs5$ and $9\farcs5$ radius had been predicted from an analysis of ^{12}CO $(1-0)$ line spectra (Whiteoak et al. 1990). Dahlem et al. (1993) saw only one "ring" in higher resolution CO $(2-1)$ data. This ring has the radius of the inner ring identified by Whiteoak et al. (1990), but the velocity of the outer ring. Dahlem et al. (1993) suggested that there is one ring with radially varying excitation conditions. Bergman et al. (1992) support this interpretation, based on a careful analysis of ^{12}CO and ^{13}CO $(1-0)$ spectra. They report a dependence of the intensity ratio of these isotopomers on radial velocity and suggest that this may be caused by systematic variations in the shielding of individual molecular clouds forming a ring at a radius 200 pc ($12''$). Obviously their proposed ring is what we see as the red and blue maxima. From the contour plot of the ^{12}CO $3-2$ intensities alone (Fig. 3), it is not possible to reconstruct the face-on appearance of the molecular complex. While a ring is plausible, it could as well be a molecular bar, a disk, a spiral, or even two independent molecular hotspots (see the discussion in Paper I).

Within $\pm 5''$ around the nucleus, maximum velocities change from ~ -215 km s^{-1} to $\sim +215$ km s^{-1} with respect to the systemic velocity of $v_{\rm LSR} \sim 555$ km s^{-1} (Ott 1995). This is slightly larger than maximum velocities a few arcminutes away from the nucleus of $\sim \pm 190 - 200$ km s^{-1} found from CO $J = 2-1$ and H I studies (Ott 1995). This may in part be due to the larger intrinsic linewidths of molecular clouds in the central region of NGC 4945. From the data presented by Ott (1995), the "rotation curve" has a minimum in velocity at about $90''$ from the nucleus. This could have two reasons: firstly, an absence of gas that could trace the velocities expected from a normal, i.e. steadily rising, rotation curve; secondly, significant noncircular motions in the central parts of NGC 4945. The latter explanation has been proposed to explain the position velocity diagrams of CO emission from the central region of the Milky Way (e.g. Binney et al. 1991) and of the edge-on spiral NGC 891 (García-Burillo & Guélin 1995).

4.3. Nuclear rotation curve and dynamical mass

In Paper I we have used the relation

$$\frac{M_{\rm dyn}}{\rm M_\odot} = \eta\, 232 \left(\frac{R}{\rm pc}\right)\left(\frac{v_{\rm R}}{\rm km\,s^{-1}}\right)^2, \tag{1}$$

to determine the dynamic mass $M_{\rm dyn}$ from the maximum velocity $v_{\rm R}$ at a distance R of the center of mass. For a spherically symmetric mass distribution, which may approximately hold for the bulge of NGC 4945, $\eta = 1$ (Lequeux 1983). As for NGC 253 (Paper I) we determine the values of v by subtracting/adding 30 km s^{-1}, the probable intrinsic half-intensity line width of molecular clouds in galactic nuclei to the lowest contours seen in the red/blue part of our position velocity plot (Fig. 5). This procedure can be used for radii outside the red/blue maxima. It is further assumed that the central maximum coincides with the kinematical center of NGC 4945, which is suggested by its almost systemic velocity. We then find that the dynamical mass in the inner R = 100 pc is $8\,10^8$ M$_\odot$; for $R \leq 200$ pc: $1.4\,10^9$ M$_\odot$; for $R \leq 400$ pc: $\sim 2.5\,10^9$ M$_\odot$ and for $R \leq 600$ pc: $\sim 3\,10^9$ M$_\odot$. These values are within 20% of the dynamical masses derived in Paper I for NGC 253.

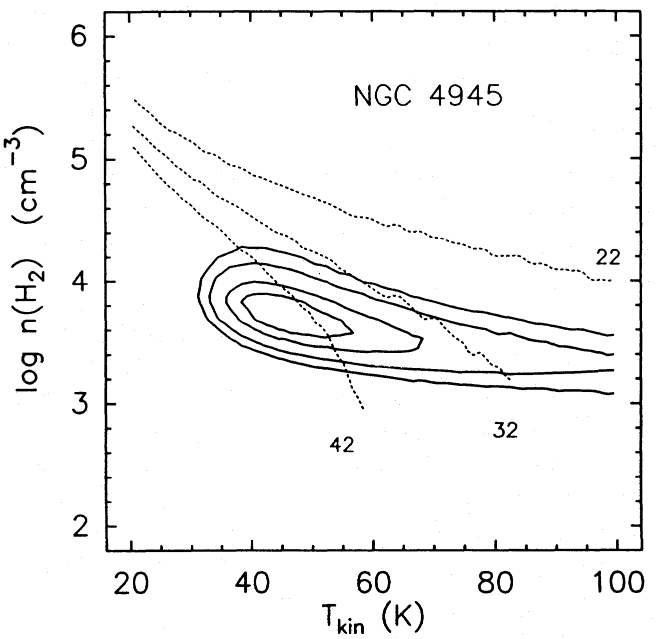

Fig. 8. Reduced χ^2 (thick contours: 0.25, 0.5, 1, 1.5) for a model fit to the line intensities of the ^{12}CO and ^{13}CO 1 − 0 to 3 − 2 lines (see Table 2, values for 24″ resolution) for a range of H_2 densities and kinetic temperatures. The assumed n(CO)/(dv/dr) is 0.032 cm^{-3}/(km s^{-1} pc^{-1}). The dashed contours denote model predictions for the HCN(1 − 0)/HCN(4 − 3) ratio (observed value: ∼ 32). Assumed n(HCN)/(dv/dr): 6 10^{-6} cm^{-3}/(km s^{-1} pc^{-1}).

4.4. Excitation conditions and the physical state of the gas

We have used a large velocity gradient (LVG) radiative transfer model (see e.g. Mauersberger et al. 1995) to compute CO and HCN line intensities for a wide range of parameters. We have compared the model results with the measured values at a resolution of 24″ (Table 2) using a reduced χ^2 test (Bevington & Robinson 1992). The ^{12}CO (1 − 0) line intensity for a 24″ beam was obtained by multiplying the measured signal (beamsize, θ_b: 43″) with $T_{\rm MB}(2-1;\theta_b = 24'')/T_{\rm MB}(2-1;\theta_b = 43'')$. The ^{13}CO $J = 1-0$ intensity in a 24″ beam was extrapolated assuming that the ^{12}CO/^{13}CO intensity ratio is the same at 43″ and 24″ resolution. The beam dilution factor, f, was determined from the predicted $T_{\rm B}$ and the observed $T_{\rm MB}$ temperatures. The ^{12}CO $J = 2-1$ line was used as a reference to estimate line brightness temperatures of the other transitions observed. It was assumed that each $T_{\rm MB}$ value has an uncertainty of 20%. The results of the χ^2 test are shown in Fig. 8.

A good fit to the CO data can be obtained for a column density parameter n(CO)/(dv/dr) of 0.032 cm^{-3}/(km s^{-1} pc^{-1}) (corresponding to N(CO)/Δv = 9.8 10^{16} cm^{-2}/(km s^{-1})), ^{12}CO/^{13}CO = 50, a kinetic temperature ∼ 45 K and an H_2 density of 5000 cm^{-3}. In our best fit model, the $J = 1-0$ line of ^{12}CO is only moderately optically thick (τ ∼ 1.6); while the 2 − 1 and 3 − 2 lines are optically thicker (τ = 6 and 9). Other combinations of $n(H_2)$ and $T_{\rm kin}$ can also reproduce the observed data, e.g. ($n(H_2)$, $T_{\rm kin}$)= (2500 cm^{-3}, 90 K). The excitation parameter of the gas, $T_{\rm kin}\sqrt{n({\rm H_2})}$ is lower than toward NGC 253 and more similar to that of M 82 (see Güsten et al. 1993). Our CO $J = 3-2$ data exclude densities as low as $n(H_2)$ ∼ 200 cm^{-3} which were suggested by the clumpy nuclear ring model of Bergman et al. (1992). The gas densities obtained with our model ($n(H_2) > 2000$ cm^{-3}) exceed the mean stellar densities (as derived from the results in Sect. 4.3) in the inner $R \leq 200$ pc (40 M$_\odot$ pc^{-3}, corresponding to $n(H_2)$ of 850 cm^{-3}). Thus the molecular gas can exist in clouds which are stable against tidal disruption.

With $T_{\rm MB,CO\,(3-2)}$ ∼ 5 K and $T_{\rm B,CO\,(3-2)}$ ∼ 27 K predicted from the best fit model, the area filling factor with respect to a 15″ beam is roughly 20% *at a given velocity*. If the gas in the nuclear region consists of the three clouds which can be identified from our position velocity plot (Fig. 5), each would have a diameter of ∼ 7″.

Henkel et al. (1994) observed a number of CO isotopic substitutions and high density tracing molecules. From the line shapes of high density tracers, they conclude that high density gas (≥ 1000 cm^{-3}) coexists with the CO emitting clouds but that there are differences in the excitation along the observed structures. The $J = 4-3$ line of HCN has a critical density as high as ∼ 10^7 cm^{-3}. Toward the bulge of NGC 4945, it is much weaker than the 1 − 0 line (Henkel et al. 1994). Assuming that the HCN emission has a size which is comparable to that of the CO (3 − 2) line (12″) and correcting for the different beam sizes employed, we find I(HCN(1 − 0))/I(HCN(4 − 3)) = 32. Assuming that HCN is a factor of ∼ 5000 less abundant than CO (Irvine et al. 1987), we can predict the HCN(1 − 0)/HCN(4 − 3) line ratio (see Fig. 8). The observed ratio of 32 is best reproduced if densities or temperatures are slightly higher than those of the CO emitting gas, although with the parameters from our best model to the CO data, the HCN line ratio can be reproduced within its error limits. While the HCN $J = 1-0$ line is predicted to have a high optical depth (τ = 8), the optical depths of the 3 − 2 and 4 − 3 lines are much smaller than 1. Mauersberger et al. (1990, 1995) pointed out that there is a large range of gas phases with different densities in the central region of the starburst galaxy NGC 253 traced by molecular transitions with different critical densities. Aalto et al. (1995) reached a similar conclusion from CO studies of other starburst galaxies. From the available data, this is less mandatory for NGC 4945.

4.5. The gas mass

Several tracers of molecular mass have been proposed for galactic and extragalactical molecular cloud cores. Among these are the intensities of the ^{12}CO lines, of the optically thin CO isotopomers, and of the thermal dust emission. An extensive discussion can be found in the Appendix of Paper I (see e.g. their Table 3).

From our best model for the observed data (Sect. 4.4), the $N(H_2)/(\int T_{\rm MB}({\rm CO}){\rm d}v)$ conversion factor is 3.2 10$^{19}(\frac{X({\rm CO})}{10^{-4}})^{-1}$ cm^{-2}/(K km s^{-1}) for the CO 2 − 1 line (X: relative abundance of CO). (The conversion factor for the 1 − 0 line is less well determined but has a similar value). From the observed line intensity in the central 24″ beam and assuming that the CO abundance is similar to the value found in the local disk, this results in a beam averaged H_2 column density of $3\,10^{22}$ cm^{-2} and a total gas mass in the inner 24″ of $1.4\,10^8\,M_\odot$. Since the area filling factor is $\sim 20\%$, the source-averaged column density is $1.5\,10^{23}$ cm^{-2}. This is less than the value estimated from GINGA X-ray observations toward the line-of sight to the nucleus of NGC 4945 ($N(H_2) \sim 2.5\,10^{24}$cm^{-2}; Iwasawa et al. 1993). It is probable that the X-ray absorption is due to a circumnuclear cloud which is much smaller than our beam and whose physical parameters are not representative for the molecular gas in the bulge.

Millimeter wavelength dust continuum is an alternative tracer of the gas mass. The 1.3 mm flux density in a 24″ beam is 0.75 Jy (Chini 1990). We can estimate the contribution of the ^{12}CO and ^{13}CO $(2-1)$ lines to the flux density contained in a 50 GHz wide bolometer bandpass to be 0.36 Jy. This means that the contribution of the CO lines alone to the "continuum" flux density is about as strong as the dust continuum, which contributes 0.39 Jy. If the metallicity is three times higher than in the solar neighborhood (a value which may be typical for many galaxies, see Vila-Costas & Edmunds 1992), we find a gas mass of $6\,10^7\,M_\odot$, using the relation from Table 3 in Paper I, and assuming $T_{\rm dust} = 30$ K (Ghosh et al. 1992).

Gas masses estimated from our CO model and from dust emission are both much lower (by factors of 6–14) than the value of $8.7\,10^8\,M_\odot$ obtained from a straight-forward use of the $N(H_2)/I_{\rm CO}$ conversion factor of Strong et al. (1988) (corrected for a small calibration error; see Bronfman et al. 1988). Similar discrepancies have been reported for an increasing number of galactic bulge regions: NGC 891 (Guélin et al. 1993), M 51 (Guélin et al. 1995), NGC 253 (Paper I), and the Milky Way (Sodroski et al. 1995 and references therein). The standard value of $N(H_2)/I_{\rm CO}$ has been determined from clouds in the local Galactic disk whose properties are different from those in the bulge regions of galaxies and reasons why this value might be too high for many bulge regions are discussed in Paper I. One way to reconcile the mass estimates from our CO model and dust on one hand, and estimates from a standard $N(H_2)/I_{\rm CO}$ ratio on the other hand is to assume that the metallicity (and, hence, the dust-to-gas ratio and the relative CO abundance) is a factor of ~ 5 *lower* near the center of NGC 4945 (and other bulge regions where there is a similar discrepancy) than in the solar neighborhood. We consider such a scenario as very unlikely for the starburst nucleus of a galaxy; it would require that the gas is essentially unprocessed and originates from the halo.

4.6. Gas fraction and star forming efficiency

Asuming that the gas mass is $\sim 1.4\,10^8\,M_\odot$ as determined from our CO model, the gas in the central 24″ contributes as much as 10% of the total mass in that region.

With the gas mass deduced from our CO model and an infrared luminosity of $2\,10^{10}\,L_\odot$ (Brock et al. 1988), a "star forming efficiency" of $\sim 140\,L_\odot/M_\odot$ is found for the nuclear region. This value is very high compared to normal spiral galaxies $\sim 5\,L_\odot/M_\odot$ and also for Markarian galaxies ($\sim 90\,L_\odot/M_\odot$) (e.g. Young & Scoville 1991, Chini 1995). Note, however, that in most cases, the gas mass has been derived from ^{12}CO $(1-0)$ lines with the standard $N(H_2)/I_{\rm CO}$ conversion factor derived for the Galactic disk. If it can be shown that the conversion factor is lower than the local value toward the centers of many galaxies, such high "star forming efficiencies" may turn out not to be as unusual as previously thought. Data of high spatial resolution (of order 100 pc) are required for such estimates, and one has to account for the possibility that some fraction of the infrared luminosity may not arise from newly formed stars but from a compact nuclear object (Iwasawa et al. 1993).

5. Conclusions

We have mapped the inner 80″ × 80″ of the Seyfert/starburst galaxy NGC 4945 in the $J = 3-2$ transition of ^{12}CO with a resolution of 15″. Our main conclusions are:

1. ^{12}CO $J = 3-2$ emission is concentrated in a central region of FWHP size 11.″5 (200 pc). From position velocity plots, the molecular complex shows three maxima, located at offsets 0″ and ±5″ from the kinematical center. From the size and orientation of the CO emission, this molecular complex may coincide with the 12″ × 9″ region of intense far infrared emission. The available information is not sufficient to reconstruct its face-on view, i.e. to decide whether it is a bar, a ring or a spiral.
2. The rotation curve deduced from position-velocity plots indicates a total dynamical mass of $3\,10^9\,M_\odot$ in the inner $R \leq 600$ pc.
3. From a standard $N(H_2)/I$(CO) conversion factor, the gas mass is $9\,10^8\,M_\odot$ in the inner $R \leq 200$ pc, while isotopic CO and dust emission yield gas masses of 0.6–1.4 $10^8\,M_\odot$. The latter gas masses would lead to a very high "star forming efficiency" ($\sim 140\,L_\odot/M_\odot$) which may in part be due not to violent star formation but to a compact nuclear object. The dynamical mass, the gas mass and the star forming efficiency are very similar to the values found for NGC 253 in Paper I.
4. Toward the central region of NGC 4945, the ^{12}CO and ^{13}CO lines contribute about as much to the "continuum" flux density in a 50 GHz wide 230 GHz window as the thermal dust emission.
5. The presence of the $J = 3-2$ line of CO and a tentative detection of the $J = 4-3$ line of HCN indicate that the H_2 densities in the central region of NGC 4945 exceed 2000 cm^{-3}.

Acknowledgements. We thank L.-Å. Nyman and L. Knee for their support during the observations. M. Dahlem and M. Ott made available their ^{12}CO $J = 2-1$ data of NGC 4945. We received useful comments from the referee. R.M. was supported by a Heisenberg fellowship by the Deutsche Forschungsgemeinschaft.

References

Aalto, S., Booth, R.S., Black, J.H., Johansson, L.E.B., 1995, A&A 300, 369
Ables, J.G., Forster, J.R., Manchester, R.N., Rayner, P.T., Whiteoak, J.B., 1987, MNRAS 226, 157
Altenhoff, W.J., Baars, J.W.M., Wink, J.E., Downes, D., 1987, A&A 184, 381
Bergman, P., Aalto, S., Black, J.H., Rydbek, G., 1992, A&A 265, 403
Bevington, P.R., Robinson, D.K., 1992, "Data Reduction and Error Analysis for the Physical Sciences", McGraw Hill
Binney, J., Gerhard, O.E., Stark, A.A., Bally, J., Uchida, K.I., 1991, MNRAS 252, 210
Booth, R.S., Delgado, G., Hagström, M., et al., 1989, A&A 216, 315
Brock, D., Joy, M., Lester, D.F., Harvey, P.M., Ellis, H.B., 1988, ApJ 329, 208
Bronfman, L., Cohen, R.S., Alvarez, H., May, J., Thaddeus, P., 1988, ApJ 324, 248
Chini, R., 1990, in "Sub-millimetre Astronomy", eds.: G.D. Watt, A.S. Webster, Kluwer, p.19
Chini, R., 1995, Habilitation Thesis, Jena University
Dahlem, M., Golla, G., Whiteoak, J.B., Wielebinski, R., Hüttemeister, S., Henkel, C., 1993, A&A, 270, 29
Della Valle, M., Melnick, J., 1992, A&A 257, L1
de Vaucouleurs, G., 1979, AJ 84, 1270
García-Burillo, S., Guélin, M., 1995, A&A 299, 657
García-Burillo, S., Guélin, M., Cernicharo, J., 1993, A&A 274, 123
Ghosh, S.K., Bisht, R.S., Iyengar, K.V.K. et al., 1992, ApJ 391, 111
Guélin, M., Zylka, R., Mezger, P.G., et al., 1993, A&A 279, L37
Guélin, M., Zylka, R., Mezger, P.G., Haslam, C.G.T., Kreysa, E., 1995, A&A 298, L29
Güsten, R., Serabyn, E., Kasemann, C., et al.,1993, ApJ 402, 537
Harris, H.C., Harris, G.L.H., Hesser, J.E., 1989, in: The Harlow Shapley Symp. on Globular Cluster Systems in Galaxies, IAU Symp. 126, ed.: J.E. Grindlay, A.G.D. Philip, Dordrecht, Reidel, p.205
Henkel, C., Whiteoak, J.B., Nyman, L.-Å., Harju, J., 1990, A&A 230, L5
Henkel, C., Whiteoak, J.B., Mauersberger, R., 1994, A&A 284, 17
Hesser, J.E., Harris, H.C., van den Bergh, S., Harris, G.L.H., 1984 ApJ 276, 491
Hui, X., Ford, H.C., Ciardullu, R., Jacoby, G.H., 1993, ApJ 414, 463
Irvine, W.M., Goldsmith, P.F., Hjalmarson, A., 1987, in: Interstellar Processes, eds: D.J. Hollenbach, H.A. Thronson, Reidel, p. 585
Iwasawa, K., Koyama, K., Awaki, H., et al., 1993, ApJ 409, 155
Jackson, J.M., Paglione, T.A.D., Carlstrom, J.E., Nguyen-Q-Rieu, 1995, ApJ 438, 695
Koornneef, J., 1993, ApJ 403, 581
Lequeux, J., 1983, A&A 125, 394
Mauersberger, R., Henkel, C., Sage, L.J., 1990, A&A 236, 63
Mauersberger, R., Henkel, C., Chin, Y.-N., 1995, A&A 294, 23
Mauersberger, R., Henkel, C., Wielebinski, R., Wiklind, T., Reuter, H.-P., 1996, A&A, in press (Paper I).
Mills, B.Y., Glanfield, J.R., 1965, Nat 208, 10
Moorwood, A.F.M., Oliva, E., 1994, ApJ 429, 602
Ott, M., 1995, Ph.D. Thesis, Bonn University
Rice, W., Lonsdale, C.J., Soifer, B.T., et al., 1988, ApJS 68, 91
Ruiz-Lapuente, P., Lucy, L.B., 1992, ApJ 400, 127
Sandage, A., Tammann, G.A., 1975, ApJ 196, 313
Sandage, A., Saha, A., Tammann, G.A., et al., 1994, ApJ 423, L13
SEST-Handbook, 1993, Version 1.0, European Southern Observatory
Shopbell, P.L., Bland-Hawthorn, J., Malin, D.F., 1993, AJ 106, 1344
Sodroski, T.J., Odegard, N., Dwek, E.,et al., 1995, ApJ 452, 262
Strong, A.W., Bloemen, J.B.G.M., Dame, T., et al., 1988, A&A 207, 1
Tonry, J.L., 1991, ApJ 373, L1
Tonry, J.L., Schechter, P.L., 1990, AJ 100, 1794
van den Bergh, S., 1989, A&AR 1, 111
Vila-Costas, M.B., Edmunds, M.G., 1992, MNRAS 259, 121
Whiteoak, J.B., Gardner, F.F., 1977, Australian J. Phys. 30, 187
Whiteoak, J.B., Gardner, F.F., 1979, Proc. Astr. Soc. Australia 3, 319
Whiteoak, J.B., Wilson, W.E., 1990, MNRAS 245, 665
Whiteoak, J.B., Dahlem, M., Wielebinski, R., Harnett, J.I., 1990, A&A 231, 25
Young, J.S., Scoville, N.Z., 1991, ARA&A 29, 581

This article was processed by the author using Springer-Verlag LaTeX A&A style file version 3.